

CERN DEVELOPMENTS FOR 704 MHZ SUPERCONDUCTING CAVITIES

O. Capatina, S. Atieh, I. Aviles Santillana, G. Arnaud Izquierdo, R. Bonomi, S. Calatroni, J. Chambrillon, F. Gerigk, R. Garoby, M. Guinchard, T. Junginger, M. Malabaila, L. Marques Antunes Ferreira, S. Mikulas, V. Parma, F. Pillon, T. Renaglia, K. Schirm, T. Tardy, M. Therasse, A. Vacca, N. Valverde Alonso, A. Vande Craen, CERN, Geneva, Switzerland.

Abstract

The Superconducting Proton Linac (SPL) is an R&D effort coordinated by CERN in partnership with other international laboratories. It is aiming at developing key technologies for the construction of a multi-megawatt proton linac based on state-of-the-art RF superconducting technology, which would serve as a driver in new physics facilities for neutrinos and/or Radioactive Ion Beam (RIB). Amongst the main objectives of this R&D effort, is the development of 704 MHz bulk niobium beta=1 elliptical cavities, operating at 2 K with a maximum accelerating gradient of 25 MV/m, and the testing of a string of cavities integrated in a machine-type cryomodule. The cavity together with its helium tank had to be carefully designed in coherence with the innovative design of the cryomodule. New fabrication methods have also been explored. Five such niobium cavities and two copper cavities are in fabrication. The key design aspects are discussed, the results of the alternative fabrication methods presented and the status of the cavity manufacturing and surface preparation is detailed.

INTRODUCTION

A first proposal for building a Superconducting Proton Linac (SPL) at CERN to replace some of the existing accelerators was reported about 17 years ago [1], with the potential for evolving towards very high beam power, which would support new physics facilities for neutrinos and/or radioactive ion beams [2]. Later, the design of the SPL evolved towards a low-power 4 GeV version (LP-SPL), with potential use as a new injector chain for the LHC, with the Linac4, presently under construction, as a low energy front-end linac, and having the potential to be up-graded to a multi-MW proton injector [3].

A synoptic of the high energy/superconducting part of the SPL is shown in Figure 1.

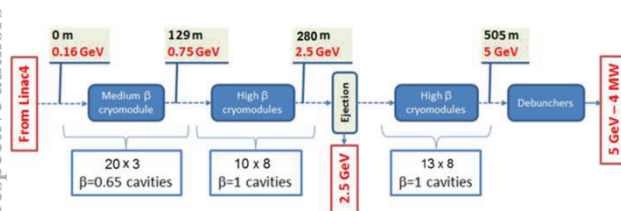


Figure 1: Schematic Layout of the SPL.

Following changes in the mid-term plan strategy at CERN, the construction of the LP-SPL has been stopped,

but the continuation of the R&D effort towards a high-power version of the SPL has been endorsed.

The motivations of the actual SPL R&D effort are multiple. One aim is to update the CERN competencies in superconducting RF. The effort is also bringing an important contribution to the upgrade of CERN infrastructure for superconducting RF like cleanroom upgrade including high pressure water rinsing facility, high power RF, diagnostics for SC RF, new electron-beam welding machine as well as an electropolishing installation. The key technologies developed in the frame of SPL R&D effort could be used for the construction of a multi-megawatt proton linac based on state-of-the-art RF superconducting technology, which would serve as a driver in new physics facilities for neutrinos and/or Radioactive Ion Beam (RIB). A tentative layout of a neutrino factory complex on the CERN site is sketched in Figure 2.



Figure 2: Draft layout of a neutrino factory at CERN.

The technologies developed will also preserve the possibility of new injectors for the future accelerators chain upgrade at CERN. Last but not least, SPL R&D presents synergy with other possible applications at CERN (LHeC electron linac, LEP-3) as well as outside CERN (ESS, ADS) towards which SPL developments could also be transferred.

As one of the priorities of this program, 704 MHz bulk niobium elliptical cavities are under development and will be tested in a fully equipped cryo-module (CM) at CERN by the end of 2015.

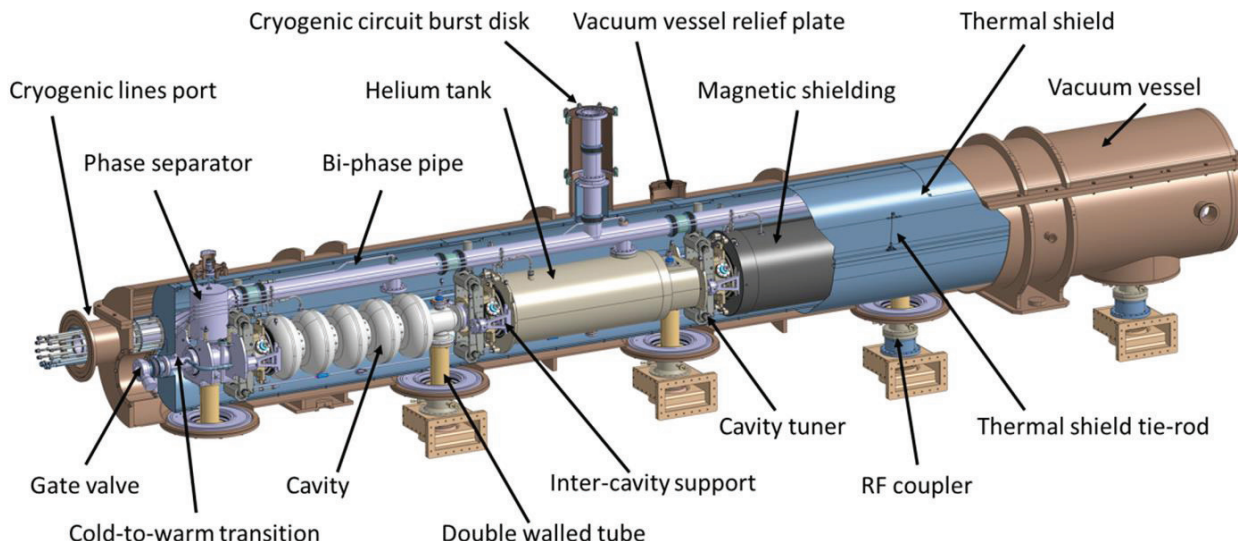


Figure 3: General Assembly View of the SPL Short Cryo-module (courtesy of IPN Orsay).

CRYO-MODULE

Amongst the main objectives of this effort, are the development of 704 MHz bulk niobium beta=1 elliptical cavities operating at 2 K and providing an accelerating field of 25 MV/m, and the test of a string of cavities integrated in a machine-type cryo-module. In an initial phase, only four out of the eight cavities of the SPL cryo-module (Figure 3) will be tested in a half-length cryo-module developed for this purpose, which nonetheless preserves the main features of the full size cryo-module [4, 5]. The four cavities, made in bulk-niobium, are housed independently in a stainless steel helium tank designed to match the tuning requirements when making use of the CEA-Saclay lever-arm type tuners. This cryo-module is being developed in the frame of a collaboration between CERN and the French institutes CEA-Saclay and IPN-Orsay.

Innovative Concept

To keep the potential heat sources in the cryo-module small, the novel SPL cavity supporting scheme does not rely on tie-rods or space frame: it only consists of the external conductors of the main RF power couplers and inter-cavity supports. The innovative concept featuring the main RF coupler acting also as the main mechanical support of the cavities, has now evolved to a mature design which is detailed in [6] and illustrated in Figure 4.

CAVITY

The SPL superconducting accelerating cavities are five-cell standing wave structures whose fundamental TM mode has a frequency of 704.4MHz. Two versions have been developed. The beta = 1 version, based on a development from CEA-Saclay [7], has an active length of about 1m. The = 0.65 version, developed by IPN Orsay [8] is correspondingly shorter. The cryo-module under development at CERN will host, in an initial phase, four

$\beta=1$ cavities that will be tested together as they would operate in a machine-type cryo-module.

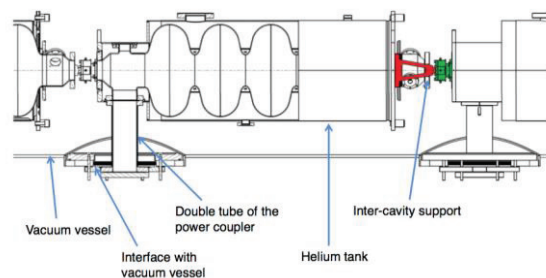


Figure 4: Double walled tube of the power coupler as supporting system.

The main design properties of the $\beta=1$ cavities are summarised in Table 1, for a 50 Hz pulsed operation, 20 mA current and 0.8 ms beam pulse length.

Table 1: $\beta=1$ Cavity, Main Design Properties & Operation

Property	units	Value
Cavity material	-	bulk niobium
Gradient	MV/m	25
Quality factor* Q_0	-	$5 \cdot 10^9$
R/Q	Ohms	570
Operating Temp.	K	2
Cryo duty cycle	%	8.22
Dynamic heat load	W	20.4

*worst case assumption

The cavities are made from solid niobium, and are bath-cooled by super-fluid helium at 2 K. Each cavity is equipped with: a helium tank; a tuning system as designed

by CEA-Saclay [9]; a coaxial RF power coupler [10]; a pickup probe; and two higher-order mode (HOM) couplers, one on each side [11]. Depending on the beam characteristics, the HOM couplers may be omitted under certain conditions, and they will only be installed in a second phase of the cryo-module tests.

The superconducting resonators are fabricated from bulk niobium sheets by electron-beam (EB) welding of spun half cells. The tubes for the beam pipes and the coupler ports are made by back extrusion and are joined to the cavity by EB welds. Figure 5 presents the cavity together with its helium tank, the main coupler, the HOM coupler, the tuner and the cold magnetic shielding, in the configuration that will be tested at CERN in the cryo-module.

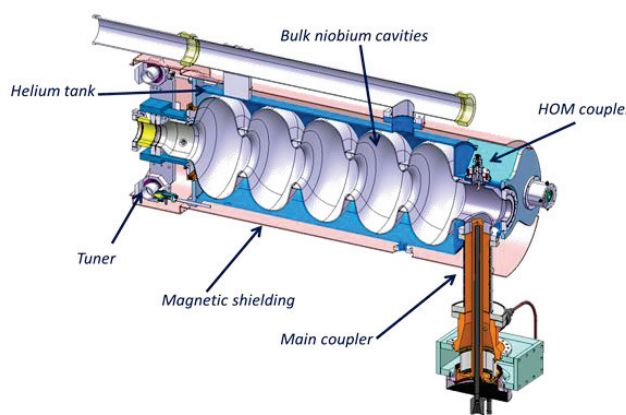


Figure 5: SPL $\beta=1$ cavity with helium tank, tuner, main coupler, HOM coupler to be tested at CERN in cryo-module.

The cavity is asymmetrical: the drift tube at the right of the figure has a diameter of 140 mm, necessary to receive the fundamental power coupler which has a 100 mm diameter. The second drift tube, hosting the tuning system, has a 130 mm diameter. The diameter is reduced at both sides to 80 mm for the connection between two adjacent cavities, provided by flanges.

The mechanical design of the cavities ensures their safe use under maximum loading condition during its entire lifecycle, and minimizes their sensitivity to the Lorenz force during operation in the pulsed mode [12].

Two copper cavities, with the same geometry as the niobium cavities, have been manufactured at CERN to be used for ancillary tests, for real-scale HOM measurements, to set all the manufacturing parameters and to identify possible difficult steps. One monocell and four five-cell niobium cavity are manufactured by industry (Research Instruments, Germany), and one five-cell cavity is manufactured at CERN.

The material specification and manufacturing process for the cavities were detailed in [12]. We will focus in the next paragraph on some additional developments as well as challenges we had to face during the manufacturing process.

Material

High purity niobium (RRR > 300) in the form of sheets and tubes has been supplied by two firms with confirmed experience working with high purity niobium: Plansee Metal GmbH (plates and tubes) and Ningxia Orient Tantalum Industry Co (plates only). Once arrived at CERN, the quality control of the supply consisted in the characterization of one random plate of each batch to assess the conformity with the technical specification specially written for the procurement of this material.

After non-destructive testing was proven successful (no continuity faults and attenuation < 20 %), mechanical testing was carried out at room temperature, yielding the results summarised in Table 2, 3 and 4.

Table 2: Mechanical Properties from Tensile Tests in Rolling Direction, Supplier A Plates

Plate	UTS [MPa]	A %	Rp 0.2 [MPa]	HV10
A plate 1	166	56.0	67	43
A plate 2	180	54.8	74	43
A plate 3	166	51.6	66	48
A plate 4	167	60.0	75	50
A plate 5	166	48.7	71	47

Table 3: Mechanical Properties from Tensile Tests in Transverse Direction, Supplier A Plates

Plate	UTS [MPa]	A %	Rp 0.2 [MPa]	HV10
A plate 1	168	45.8	71	45
A plate 2	173	51.9	64	44
A plate 3	165	54.5	73	49
A plate 4	166	48.9	72	49
A plate 5	168	56.6	72	46

Table 4: Mechanical Properties from Tensile Tests, Supplier B Plates

Plate	UTS [MPa]	A %	Rp 0.2 [MPa]	HV10
B plate RD	202.6	43.1	129.0	64
B plate TD	205.1	50.4	115.0	62

Supplier A material is fulfilling the specification (UTS > 140 MPa A% > 30%, 50 MPa < Rp0.2 < 100 MPa and HV10 < 60). The material from supplier B is also fulfilling the specification in terms of UTS and elongation at break, but it has slightly superior hardness and yield strength. This fact can have consequences during the

spinning of the half cells and also for the tuning operations.

Additionally, tensile tests at 4.2 K were carried out on two samples coming from Supplier A. The stress - strain curve of the sample extracted in the transverse direction can be seen in Figure 6, exhibiting the so called discontinuous plastic flow or serration just after the elastic limit. The results for both tests are summarized in Table 5.

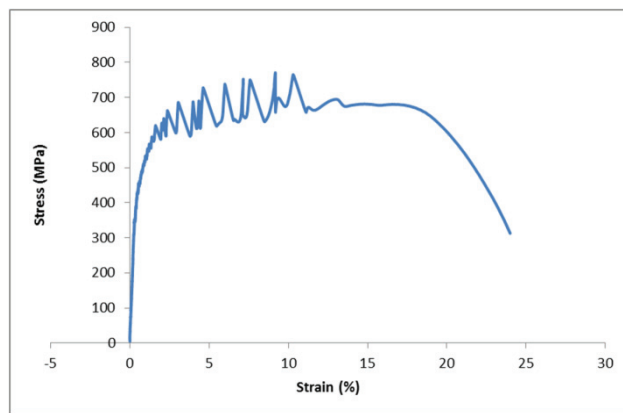


Figure 6: Tensile test on niobium sample from Supplier A plate 2 at 4.2 K.

Table 5: Mechanical Properties from Tensile Tests at 4.2 K

Sample	UTS [MPa]	A %	Rp 0.2 [MPa]
A plate 2 in TD	771	24.0	480
A plate 2 in RD	808	22.5	520

For the grain size, it was evidenced the difficulty of controlling it with a material of such a high purity and hence such a low number of centres for nucleation of the grains. The results of the grain size measurements together with a metallography from each firm are shown in Table 6 and Figure 7.

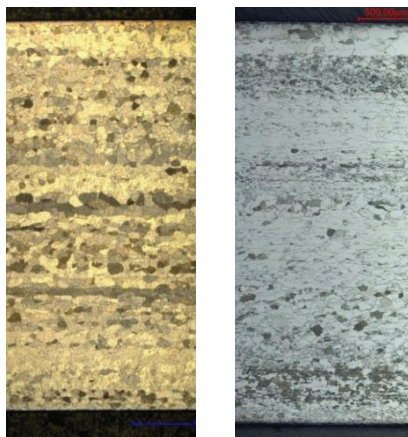


Figure 7: Metallographic observation of Supplier A plate 2 (left) and Supplier B (right).

Table 6: Summary of the Metallographic Observations of the Material from Supplier A and Supplier B

Plate	Homogeneous	G _{min}	G _{max}	Ø _{min} [µm]	Ø _{max} [µm]
A plate 1	Yes		6.0		44.9
A plate 2	Yes		5.3		58.5
A plate 3	No	3.0	4.3	127.0	80.2
A plate 4	Yes		5.0		63.5
A plate 5	Yes		5.3		58.5
B plate	No	6.5	9.5	37.8	13.3

For a better understanding of the behaviour of the material when submitted to stress and in particular to assess the increase of the strength of the material due to plastic deformation, the strain hardening coefficient (n) was calculated by representing real strength vs real strain in a logarithmic scale (Figure 8) and calculating the slope of the curve as established in ASTM E646 – 07.

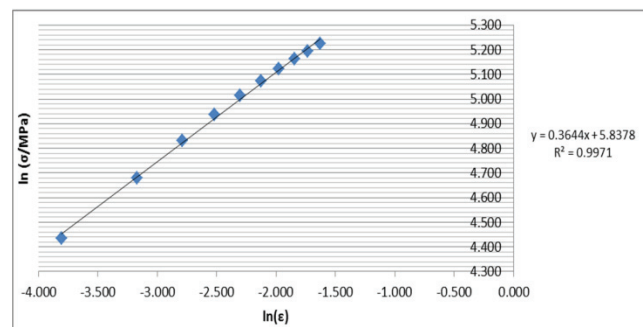


Figure 8: True stress vs. true strain curve in a logarithmic scale used for the determination of n .

The values were once again calculated for a plate of every batch (only for Supplier A) and the results show to be very homogeneous, as summarized in Table 7.

Table 7: Summary of the n values calculated from tensile tests for the plates of Supplier A

Plate	n value
A plate 1	0.37 ± 0.01
A plate 2	0.35 ± 0.02
A plate 3	0.35 ± 0.02
A plate 4	0.32 ± 0.01
A plate 5	0.36 ± 0.01

One of the main stages of the quality control consisted in the measurement of the residual resistivity ratio (RRR), capital for a good performance of the cavity. The values obtained are summarized in following Table 8.

Table 8: RRR Measurements at 10 K ⁽¹⁾ or 9.5 K ⁽²⁾

Plate	Rolling	Transverse
A plate 1 ⁽¹⁾	319	330
A plate 2 ⁽¹⁾	317	324
A plate 3 ⁽¹⁾	287	283
A plate 4 ⁽¹⁾	259	260
A plate 5 ⁽¹⁾	285	276
B plate ⁽²⁾	275	280

For the correct interpretation of these values, it has to be kept in mind that the measurements at cryogenic temperature were done at 10 K for the samples of Supplier A and at 9.5 K for the ones of Supplier B. If going strictly to the definition (ratio between resistivity at room temperature and resistivity at 4.5 K), all the values would be above the required 300.

In order to complete the quality control of the material and for improving the visual inspection of superficial defects and/or inclusions of foreign material, anodising tests were proposed. Anodising is an electrolytic passivation process used to increase the thickness of the natural oxide layer found in the surface of metals. By controlling the parameters of the electrolytic process, different surface colours can be obtained (Figure 9), and this is the principle which underlies for the use of anodising as a process for the visual inspection of surfaces. With a set of controlled parameters, the colour of the niobium surface is known so that anything with a different colour can be interpreted as an inclusion of foreign material.



Figure 9: Anodised niobium at different voltages.

For our application, it was decided that the best contrast would be obtained with 10 and 20 V, so for every type of inclusion, two samples were contaminated with inclusions of typical materials found in a workshop and some of the typical impurities found in niobium. Samples were then anodised (Figure 10) and visually inspected.



Figure 10: Contaminated and anodised samples for visual inspection.

The result was that the inclusions appear the same size as they were originally, so, apart from a negligible gain in contrast, the detection of the inclusions was as difficult as in non-anodised samples, requiring in most of the cases the use of a microscope to identify them. For this reason, and because the risk of damaging the plates during handling was higher than the advantages in the detection of superficial foreign inclusions, it was decided that anodising will not be used for the quality control of the SPL material.

Manufacturing

Spinning has been chosen as shaping technique for the half-cells as can be observed in Figure 11.



Figure 11: Niobium cavity extremity and half-cell done by spinning.

Copper half-cells have been machined by turning the entire inner surface (RF surface) after the spinning process, resulting in average final shape accuracy as good as ± 0.15 mm. The inner part of the niobium half-cells were not machined after spinning since the resulting final thickness would have been too low for mechanical integrity of the cavity during transients and operation conditions. Sheets thicker than the available ones would have been necessary. While extremely good shape accuracy was achieved for copper cavities, achieving good tolerances for the niobium half-cells was a significant challenge. The shape accuracy obtained for niobium is up to the millimetre range, and alternative shaping techniques are under study for future manufacturing optimisation.

Spinning has also been used to shape the conical part of the end groups for the cavities manufactured at CERN (two copper and one five-cell niobium) as shown in Figure 11. The end groups for the niobium cavities produced by RI were manufactured from seamless niobium tubes described below. Stainless steel flanges (316 LN) are then assembled by brazing. The half cells are electron beam welded with full penetration at the iris (Figure 12) both from inside and outside in order to decrease the energy deposition. A cross section of a copper weld at the iris can be seen in Figure 13.

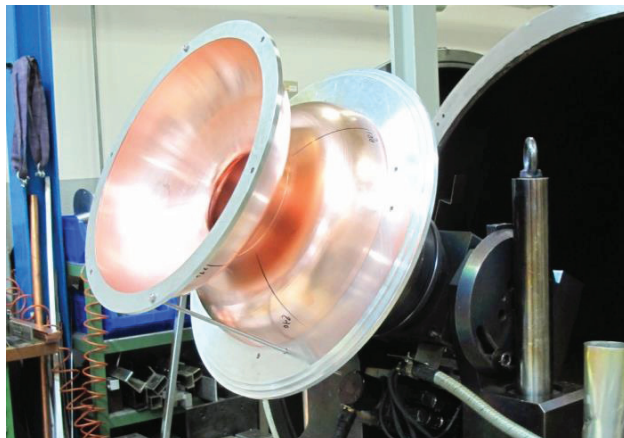


Figure 12: Layout of the pieces for electron beam weld of the iris.

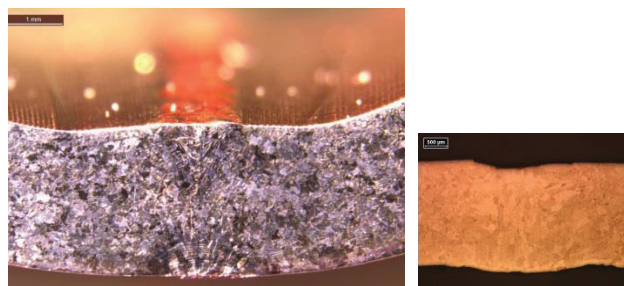


Figure 13: Metallography of a weld cross section of the iris (left) and equator (right).

Reinforcement rings are then fully penetration welded with a weld of 2.4 mm depth. Then the equatorial welds are carried out. The equatorial weld is the most difficult as it has to be fully penetrated of 2.4 mm, done only from the outside, and present a very smooth surface in the inside. A cross section of one copper weld at the equator can be seen in Figure 13.

Welding suitable settings for the requirements of the different niobium linear and circular welds are also studied with satisfactory results as presented in Figure 14.

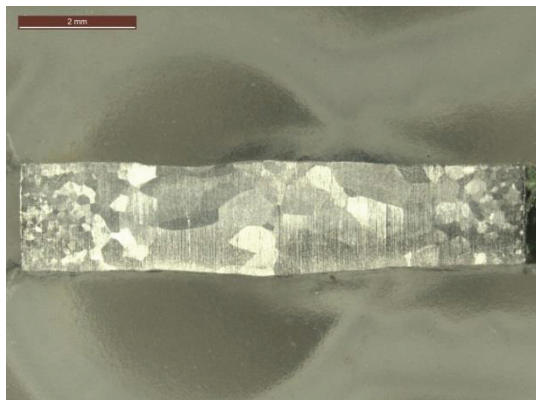


Figure 14: Metallography of a cross section of a linear niobium weld test presenting no defects.

Challenges with Seamless Niobium Tubes

Seamless niobium RRR300 tubes have been used to manufacture the cavity extremities as well as coupler ports. The combination of purity and tight dimensional tolerances made the production of these parts a technological challenge for the supplier. The tolerances were hardly achieved in the first trials, what translated to important delays in the reception of the material. On top of that, during different steps of the manufacturing, material discontinuities were detected, reason why a deeper investigation was carried out to try to better understand their origin.



Figure 15: Metallographic observation of a defect found in the inner surface, submitted to electropolishing (left), and in the outer surface, not submitted to electropolishing (right).

Two different pieces were studied, both coming from the same supplier. It has to be underlined that US tests were carried out in all the tubes and no remarks were done. The first part which was studied in more depth was a cut-off tube coming from the monocell cavity which, after an electropolishing treatment, showed evidence of discontinuities on its inner and outer surfaces. After x-ray analyses confirmed lack of material all around the tube, metallographic examinations of the cross section of 2 inner discontinuities together with an external one were carried out.

The study of several defects of the internal surface shows that they are confined in a depth of around 100 µm, presenting a round aspect in their edges (Figure 15). This last feature is most distinctive when comparing them with the defect observed in the outer surface (Figure 15). The interpretation that can be derived from this comparison is that superficial discontinuities, present in the tube due to its production process and/or to scratches due to handling operations, have been enlarged by chemical processes, especially the electropolishing.

Other piece which was analysed comes from a tube of 99.8 mm internal diameter. The defect was detected by the manufacturer of the cavities after machining of the surface (Figure 16). A cross section of the defect was ground and polished to a mirror – like finishing. It was then etched with #160 etchant according to ASTM E407 – 93 to reveal the grain boundaries. Observations showed that the defect progresses in a transgranular way to a depth of approximately 500 µm (Figure 17).



Figure 16: Material defect observed after machining of the surface.

In order to have more detailed information of it, SEM observations of the cross section of the defect were carried out in the same cross section mentioned above. As it can be seen in Figure 18, the branches which grow from the defect have the aspect of chemical dissolution.

From the results herein presented, it seems that the defect observed is an isolated and rare phenomenon of uncertain origin. From the dendritic aspect of the cross section in Figure 17 and the detailed image of Figure 18, it looks like a case of stress – corrosion cracking which will need to be studied in more detail as this kind of damage has never been documented in literature for niobium.



Figure 17: Metallographic observation of a cross section of the defect.

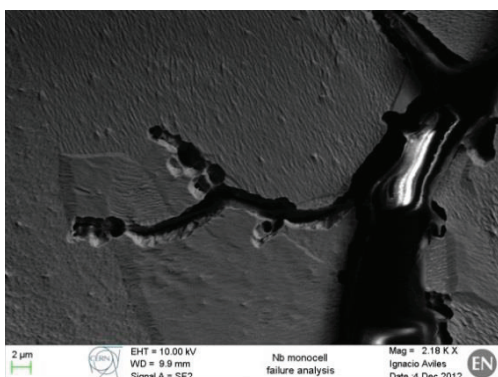


Figure 18: SEM image of one of the branches of the cross section of the defect.

For the manufacturing of the end groups, a necking – out process is carried out. It consists in perforating a series of ellipses where the different ports are placed in order to, with the help of a specially designed tooling, pull out of the tube the extra length to which the ports (with their corresponding brazed flanges) will be welded. Like this, the difficulty of the EB welding is highly decreased. The length of the axis of the ellipses is in direct relation with the final diameter of the port and the height which will be protruded from the end group in order to weld it. During this necking – out process problems of excessive deformation in the material were detected (Figure 19).

This was mainly the case for necking out from seamless tubes, the same geometry being successfully achieved when the end group was produced from sheets (rolled or spun).



Figure 19: Fractures observed after the necking – out of a port in an end group.

Material characterization was carried out even if the fracture surface indicated excessive deformation as the cause of the break. Fully recrystallized equiaxial grains were found and a hardness of 57.1 HV10 was measured, what fulfills CERN specification for RRR 300 niobium. A comprehensive analysis of the situation ended with the recalculation of the necking – out parameters in order to have the least deformation to make the EB welding possible. New trials with the optimized size of the ellipses were carried out at CERN with successful results.

Niobium to Stainless Steel Transitions

The titanium solution for helium tank material has been investigated first. Several developments have been done related to it and are reported in [12].

The stainless steel solution for the helium tank has also been investigated and represents the baseline solution for the $\beta=1$ cavities that will be tested in a cryo-module at CERN. The transition to the adjacent components in stainless steel is straightforward since stainless steel to stainless steel ConFlat flanges are extensively used at cryogenic temperature. For the transition of niobium to stainless steel, two different solutions were assessed: brazing and electron beam welding, using for both of them OFE copper as interlayer.

Brazing of niobium and stainless steel is a key technology developed at CERN which has been proven

07 Cavity design

O. Cavity Design - Accelerating cavities

successful on multiple occasions [13, 14]. Nevertheless, it was decided to study it in depth with the new available techniques and also to determine if it fulfilled the mechanical requirements intended for its use.

Before the brazing operation, an extremely careful preparation of the samples is of paramount importance. For this, a small groove of 1.1 mm diameter is machined in the flange to host the brazing metal (OFE copper). Moreover, the differences in thermal expansion coefficients call for a special layout of the pieces by inserting a stainless steel plug in intimate contact with the internal diameter of the niobium tube as in Figure 20. The reason for this is to ensure that the 20 μm of maximum clearance between the stainless steel flange and the niobium tube, capital to guarantee a good filling of the Nb – SS interface, is respected.

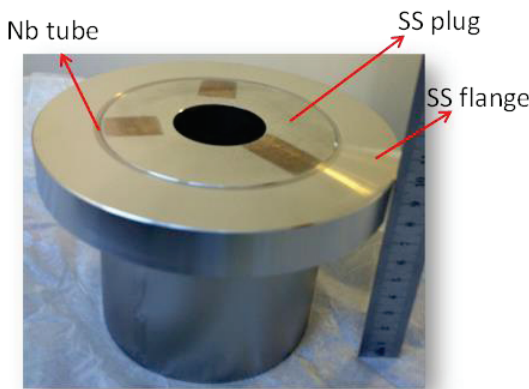


Figure 20: Layout of the pieces before the brazing operation.

The pieces are then brazed under vacuum (10^{-5} mbar) at a temperature slightly above the melting point of copper for a short period of time in order to avoid as much as possible the diffusion processes that could jeopardize the quality of the joint. After the brazing operation is finished, the plug is machined out.

Two types of tests were carried out. One oriented to determine if the joint was fulfilling the mechanical requirements for which it is designed and a second one which is more focused in a comprehensive study of the interfaces between the materials.

For the first one, ultrasonic examination was carried out to assess the continuity of the interfaces before and after mechanical loading of the joint (2 sets of 5 thermal shocks in liquid nitrogen, a heat treatment at 600 °C for 24 hours and a shear test of 3 tons, which means 10 times the actual mechanical solicitations intended for the cavity). Leak-tightness test after each ultrasonic examination was done, plus an extra analysis after the electropolishing stage. Both test campaigns produced satisfactory results, proving the high robustness and reliability of the joint.

For the second purpose, metallographic cuts of the cross section, SEM + EDS analyses together with a fractographic analysis were carried out. As it can be

noticed in Figure 21, there is a very clear affinity of the stainless steel and the copper, infiltrating the last one inside the grain boundaries of the first one thus enhancing the strength of the brazed joint. On the other hand the fact that the copper has not diffused to the niobium was rather expected as in some applications (e.g. superconductive wires), niobium is used as a diffusion barrier for copper.

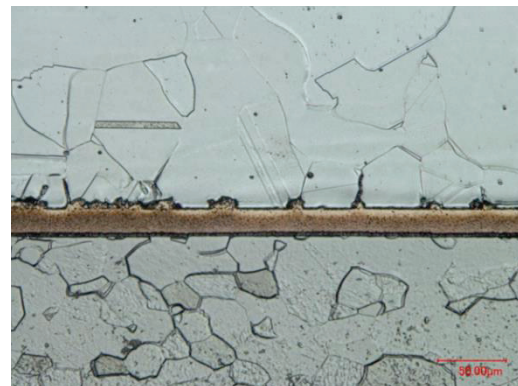


Figure 21: Metallographic observation of the brazed joint with Stainless steel on top, copper in the middle and niobium in the bottom.

When observing this interface at higher magnifications (Figure 22) with the help of the SEM, we detect via EDS analysis a layer rich in chromium and iron (Figure 23) coming from the diffusion of these elements from the stainless steel.

The fractographic analysis confirmed the formation of brittle intermetallic compounds in the mentioned interface. Figure 24 shows very clearly the characteristic faceting found in brittle fractures. This kind of behaviour was both expected and, for the mechanical requirements of the cavity, not dangerous as it was proven by the mechanical tests.

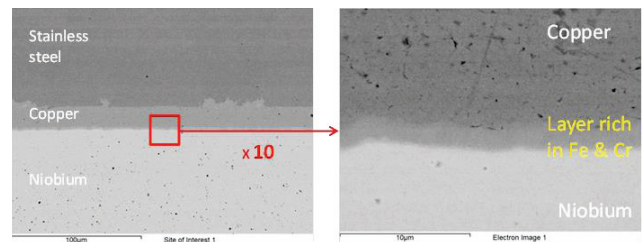


Figure 22: SEM images taken with AsB detector, more sensitive to composition of the samples.

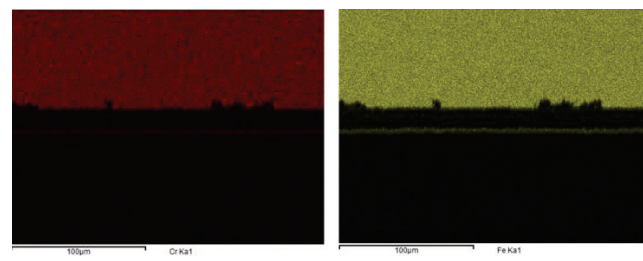


Figure 23: EDS qualitative analyses showing higher concentration of Cr and Fe in the Nb – Cu interface.

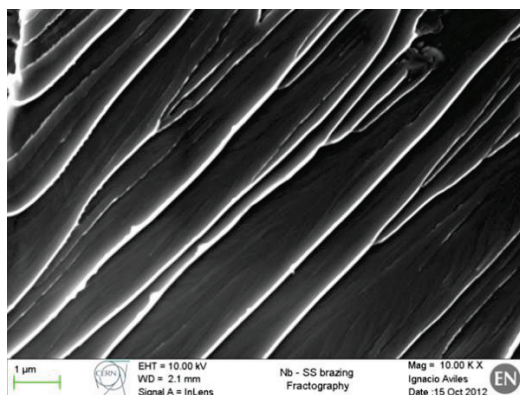


Figure 24: Fractography of the Nb – Cu interface observed in the Nb side.

In parallel to these studies which are targeted to the determination of the feasibility and usability of the junction, another important challenge which showed up was the potential detrimental effect of the buffered chemical polishing to which the cavity will be submitted.

For this study, a niobium plate was brazed to a stainless steel one using copper OFE as brazing metal, and it was then cut into 10 pieces (Figure 25) which were introduced in a chemical bath [(1:1:2) in volume of 40% HF, 65% HNO_3 , 85% H_3PO_4] under different stir and cooling conditions.



Figure 25: Nb – SS brazed samples for chemical testing.

The results revealed that, in average, 200 μm of the brazing metal were removed as a consequence of the submission of the pieces to the chemical bath (Figure 26), and in the worst case, up to 300 μm were removed.

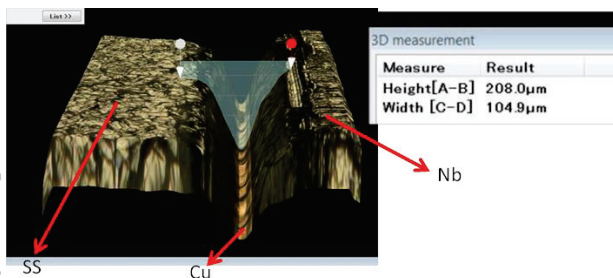


Figure 26: Nb – SS brazed samples after chemical testing.

Eventhough these figures represent roughly 2 % of the brazed surface, what is far below the specified values, it

was decided to avoid damaging the joint. To accomplish this goal, a polymer invulnerable to the chemical agents present in the bath will be used to mask the interfaces, to guarantee their integrity.

FIELD MAPPING AND TUNING OF THE SPL CAVITIES

To achieve cavity operation at the required RF frequency, there are three main steps to be followed for adjusting the cavity frequency:

- First step is during the manufacturing process, by trimming the equators of each dumb-bell at a target frequency prior to cavity final assembly.
- Second step is done at room temperature on the finished cavity and consists in tuning each cell by plastic deformation to adjust the cavity frequency as well as the field flatness in the cavity.
- The third step is adjusting the cavity frequency at operating temperature (2K in our case) using a “cold tuner” by deforming elastically the entire cavity in the longitudinal direction.

After the final equatorial welding, the five-cell cavity should have the design frequency and the corresponding field flatness of the accelerating Pi-mode within the range of the tuning machine. The flatness of the electric fields located in the cell centres is quantified by:

$$FF = 100 * \frac{v_j^{\pi} \max - v_j^{\pi} \min}{\sum_{j=1}^5 v_j^{\pi}}. \quad (1)$$

Where FF stands for the field flatness and $v_j^{\pi} \max$ indicates the electric field amplitude of the Pi-mode located in the centre of cell j ($j=1\dots5$). According to the specification the SPL cavities should achieve final field flatness below 2.5 %.

For the purpose of field distribution mapping an automated bead-pull test stand was designed and commissioned (Figure 27).

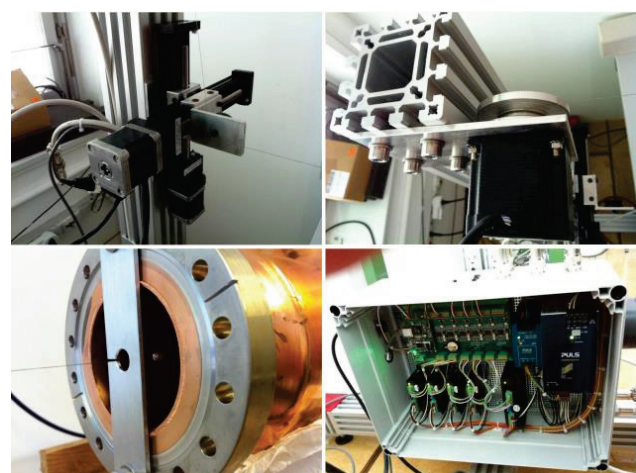


Figure 27: Automated bead-pull test stand for SPL cavities.

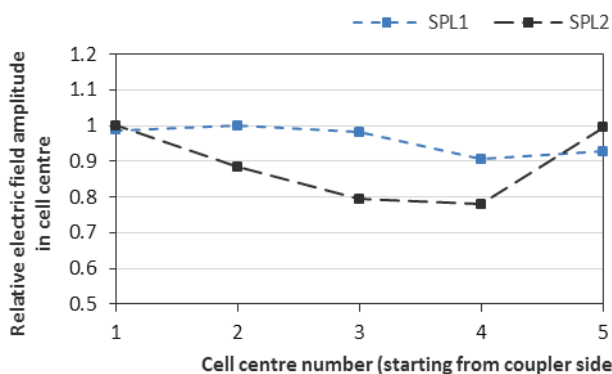


Figure 28: Bead-pull results of the SPL copper mock-ups.

The measurement method is based on Slater's perturbation theorem. Two (as-manufactured) five-cell copper cavities were tested so far (Figure 28). SPL1 has an initial field flatness of $9.68\% \pm 0.6$ meanwhile SPL2 showed a worse initial performance with $24.77\% \pm 1.1$.

The field inhomogeneity of the cavity assembly is due to mechanical imperfections resulting in individual cell shape deviations. A flat field profile can be achieved by applying a permanent mechanical deformation to each cell. For this purpose a tuning machine was developed (Figure 29) to adjust the frequency for each cell of the cavity. The tuning machine can be used together with the bead-pull test stand.



Figure 29: Tuning machine.

A method based on circuit model will be used to mathematically pre-tune the cavity hence reducing the number of iteration in tuning. The required corrections per cell can be calculated from the data collected by the bead-pull measurement of all the resonant modes of the cavity in the first band and finally can be converted to Pi-mode frequency shifts.

The bead-pull results of the copper cavities show the essential importance of quality assurance by RF measurements in the mid-process of the production chain. In case of SPL1 the ideal frequency adjustment of the dumb-bells was implemented by trimming the overall length symmetrically on both sides. In most cases the correction resulted in a shorter length compared to the design hence the dumb-bells were over-trimmed. There were no corrections for frequency in case of SPL2, the

07 Cavity design

O. Cavity Design - Accelerating cavities

dumb-bells were trimmed at the nominal length. The niobium dumb-bells will be trimmed to an intermediate frequency such that in the final assembly after tuning they will have the right length and frequency.

RF and mechanical measurements have been carried out on one copper cavity during tuning of each cell in both directions (stretching and squeezing). It resulted in relatively important dispersion in tuning sensitivity for the measured cells. The results have still to be consolidated with measurements on another cavity as well as for a larger deformation range of each cell. Figure 30 shows the measured tuning sensitivity during deformation of cell no. 4.

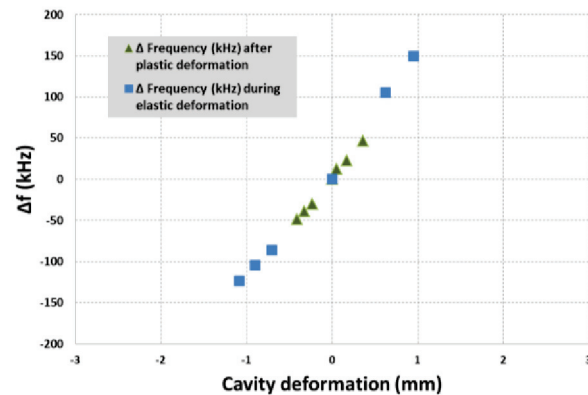


Figure 30: Measured Pi-mode frequency change vs. mechanical deformation of cell no 4.

HELIUM TANK

The helium tank contains saturated superfluid helium at 2 K cooling the cavity and allowing the extraction of the heat dissipated into the bulk niobium wall by the RF electromagnetic field, as well as the heat injected by all the adjacent components such as the main power coupler. The geometry of the helium tank has thus to allow this heat extraction while minimising the quantity of the helium to be used.

The helium tank has also a structural role since it transmits the effort applied by the tuner to the cavity, its rigidity being thus very important in the tuning process. The stiffness of the helium tank has a direct impact on the Lorentz detuning, defining the boundary conditions of the cavity. The helium tank design has been carried out to ensure a longitudinal stiffness higher than 100 kN/mm.

Detail information about the main features of the helium tank design and the related developments has been published in [12].

Five stainless steel helium tanks designed by CERN are under manufacturing by CEA Saclay and will be assembled on the niobium cavities at CERN during 2014.

COLD TUNER

Frequency variation of the cavity at cold might be induced by several factors: the remaining error of the room temperature tuning, the effect of the last chemical treatments, the differential shrinkage of materials of the

cavity, He vessel and tuner, helium pressure fluctuation as well as detuning due to Lorentz forces. The differential shrinkage of materials of the cavity, He vessel and tuner can be coped with within the tuning strategy for series cavities after the full test of the first prototype. All the remaining sources of errors have to be compensated by using a tuner able to adjust the cavity frequency at cold within a suitable tuning range.

The cavities to be installed in the SPL cryo-module will be equipped with a tuner that will be able to adjust the cavity frequency at cold within approximately 3 mm, representing a total of adjustable frequency range of about 500 kHz for our cavities. The tuner has been developed by CEA Saclay and has already been successfully used in the past [9].

Eight tuners have been manufactured by CEA and delivered to CERN, on which several tests have already been performed.



Figure 31: Tests of cavity deformation during tuning with CEA Saclay cold tuner.

Cavity deformation and tuner load distribution was measured in a dedicated set-up (Figure 31), for the total tuning range of about 2.7 mm. For the copper cavity, the measured load applied by the three rods of the tuner (Figure 32) to deform the cavity for the total tuning range is summarised in Table 9.

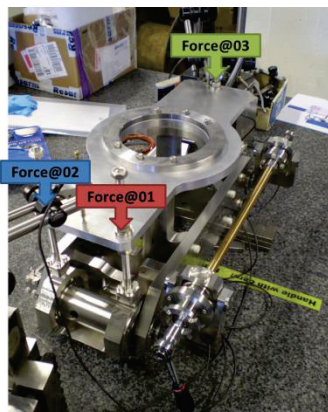


Figure 32: Load position measurement on tuner.

Table 9: Tuning Loading for Maximum Cavity Deformation

Position	Load at max range (2.7 mm)
Force 1	2.3 kN
Force 2	2.3 kN
Force 2	4.4 kN

The load values measured for the copper cavity are estimated to be slightly higher than the ones expected for the niobium cavity due to a slightly higher material thickness for copper than for niobium, the relevant material properties being significantly similar.

The total deformations of the set-up as well as each half cell deformation for the entire tuning range have been measured on a copper cavity and the results are summarised in Figure 33 and Figure 34.

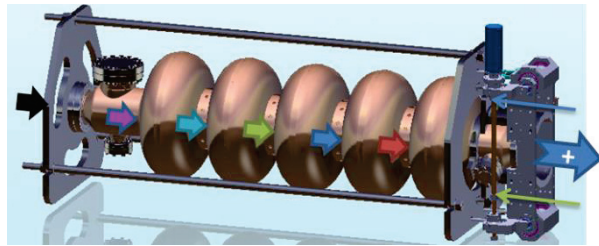


Figure 33: Measurement position.

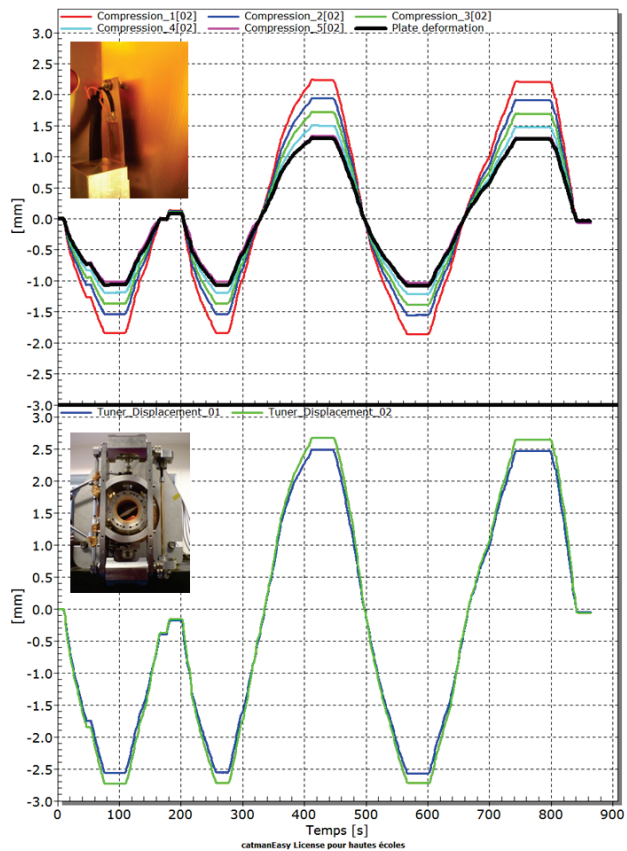


Figure 34: Measurement position.

Asymmetric deformation of each cell by up to 0.2 mm has been measured for the total tested tuning range. This asymmetry in cell deformation is probably due to the shape obtained by manufacturing (thickness variation, shape accuracy,...), as well as to the asymmetric actuation of the tuning via one rod on one side and two on the other side.

Asymmetric geometry ends, in particular different diameters for the two cut-off tubes induce asymmetric deformation of the extremity cells up to several tenths of millimetres of difference in between the two.

On the other hand, for symmetric geometries such as the three inner cells, the measured deformations differences are less than 0.1 mm.

The effect of the cavity asymmetric deformation on the cavity field profile change is planned to be measured in the coming weeks.

ELECTROPOLISHING

In preparation for the processing of the 704 MHz high-beta SPL cavities a new vertical electropolishing facility has been assembled at CERN [15]. Figure 35 presents the facility during the treatment of the niobium monocell cavity.



Figure 35: Electropolishing of niobium monocell cavity at CERN.

Working Principle

The electropolishing bath is pumped in a closed loop from a storage tank into the cavity (bottom to top) and

back. The bath temperature is monitored inside the storage tank and at the outlet on the top of the cavity; a cooling circuit inside the storage tank compensates the heating of the bath by the input process power. The bath flow is controlled and monitored at the inlet of the cavity.

Molecular nitrogen (N_2) will be introduced inside the storage tank in order to vent H_2 out, but this must be limited to avoid losing free hydrofluoric gas (HF). A secondary pump allows pumping the bath back to the storage tank as gravity flow is not possible. A demineralised water inlet is connected to the circuit in order to rinse the cavity after the electropolishing. Storage tank bath feeding and draining is done by a single point. The action is defined automatically. The DC power is supplied to the cavity by external contacts to the cavity surface (anode) and by the cathode which is placed inside the cavity.

Working Parameters

The setup was designed taking into account two interdependent parameters, bath flow and temperature. The flow should not be turbulent in any active part of the cavity in order not to disrupt the viscous layer and therefore guarantee homogeneous electropolishing conditions. It should however be sufficiently high to avoid a large temperature differential between the input and the output. Presently and for SPL beta=1 monocell, flow rate is limited to 20 lpm and the temperature difference between inlet and outlet is 1 °C.

Results

The resulting surface is bright and smooth which is proof that the SRF structures are within the limiting current range and therefore within the good electropolishing parameters. Some macrostructures are apparent, as shown in Figure 36, some are from the shaping of the SRF structure, but others are probably related to gas bubbles evolving at the surface of the SRF structure.



Figure 36: Niobium surface after 220 microns removal by electropolishing.

OPTICAL INSPECTION

The cavities control process was completed by the acquisition of an optical inspection system as shown in Figure 37. This system has originally been developed at KEK/Kyoto University and is composed of a cylinder fitting the iris of the cavity, onto which an illumination system and a CCD camera are installed. It is a powerful tool that allows the characterization of surface defects at locations hardly accessible such as the equator zones for example. Figure 38 shows the high quality image of the copper cavity equator weld.



Figure 37: Optical inspection bench.



Figure 38: Equator welding inspection of copper cavity.

CLEANROOM

Manufacturing high gradient SRF cavities requires a good control of the cleaning and assembling procedure. CERN cleanroom facilities are now about 20 years old and it has been decided to refurbish the existing SM18 test facility to comply with the required gradients of 25 MV/m. Improvement of the existing cleanroom class, construction of a new clean space and acquisition of a new high pressure rinsing system are the essential parts of the upgrade [16]. New control procedures and new instrumentations will help to monitor each step of the cleaning and assembling procedure.

This upgrade will provide a cleaner environment for high gradient component, but also, it will benefit other projects such as LHC spare cavities, by upgrading their manufacturing and assembling process.

Figure 39 presents the layout of the cleanroom facility in SM18 that will be refurbished by the end of 2013.

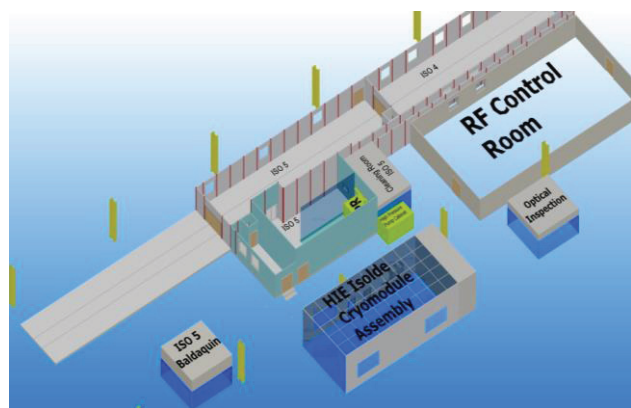


Figure 39: SM18 cleanroom refurbishment.

COLD TEST

An existing vertical cryostat has been adapted to host an SPL cavity for 2K tests for validation prior to assembly of the helium vessel. Figure 40 shows the SPL monocell installed in its vertical cold test set-up.



Figure 40: Vertical cryostat for cavity cold test.

A first cold test has been performed on the monocell cavity manufactured by RI. Even if limited performance was measured due to field emission (Figure 41), the

results are encouraging since the cavity was not fully processed when tested.

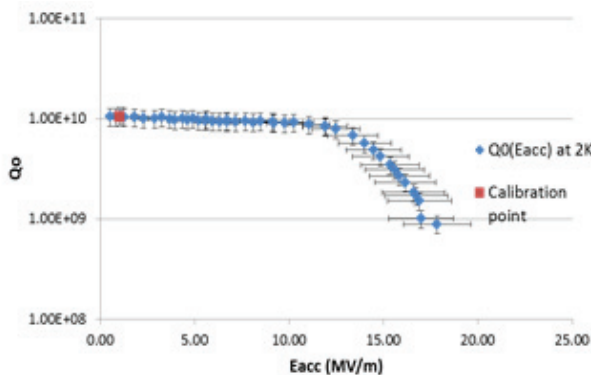


Figure 41: First test results of the monocell tests at 2K.

After the first measurement, one extremity of the cavity presenting the defect mentioned in section “Challenges with the seamless niobium tubes” was cut and repaired at CERN. The cavity has been fully re-processed and will be cold tested during the following weeks.

SUMMARY AND OUTLOOK

A string of four SPL 704 MHz $\beta=1$ superconducting cavities assembled in a so-called Short cryo-module, will be tested by 2015 at CERN in a machine-type configuration, powered by high-power RF.

Extensive studies and investment have already been done with respect to the dressed cavities, cryo-module, and equipment for cavity processing as well as needed infrastructure.

Two copper cavities and one bulk-niobium monocell have been produced. One five-cell bulk niobium cavity is under manufacturing at CERN and other four five-cell cavities will be completed by industry (RI) by end of 2013. In the frame of the SPL R&D study, innovative mechanical solutions have already been explored and a number of R&D studies are still on-going with several promising results already obtained.

REFERENCES

- [1] R. Garoby and M. Vretenar, CERN/PS/RF/Note 96–27.
- [2] M. Vretenar (ed.), “Conceptual Design of the SPL”, CERN-2000-012, <http://doc.cern.ch/yellowrep/2000/2000-012/p1.pdf>
- [3] O.Brunner et al. “Assessment of the basic parameters of the CERN Superconducting Proton Linac”, Physical Review Special Topics-Accelerators and Beams, 12, 070402 (2009).
- [4] V. Parma et al., Status of the Superconducting Proton Linac (SPL) cryo-module, these proceedings.
- [5] V. Parma et al., “Conceptual design of the Superconducting Proton Linac (SPL) short cryo-module”, SRF2011, Chicago, July 2011.
- [6] R. Bonomi et al. “SPL RF coupler cooling efficiency”, these proceedings.
- [7] J. Plouin et al. "Optimized RF design of 704 MHz beta=1 cavity for pulsed proton drivers", SRF2011, Chicago, July 2011.
- [8] G. Olry et al., Status of the medium beta=0.65 cavity development for SPL, Presentation at Joint ESS/SPL collaboration meeting 2011, 30/06-01/07 2011, CEA, Saclay (France), <http://indico.hep.lu.se/conferenceDisplay.py?confId=1066>
- [9] G. Devanz, Tuner design and performance, presentation at the 3rd SPL collaboration meeting, Nov. 11- Nov 13, 2009, CERN, Geneva (Switzerland) <http://indico.cern.ch/conferenceDisplay.py?confId=63935>
- [10] E. Montesinos, “Conceptual SPL RF Main Power Coupler design”, SLHC Project Report-0052, 16 March 2011.
- [11] K. Papke et al. “HOM Couplers for CERN SPL”, these proceedings.
- [12] O. Capatina et al. “Mechanical design considerations for beta=1 cavities”, SRF2011, Chicago, July 2011.
- [13] J.P. Bacher, E. Chiaveri, and B. Trincat, “Brazing of niobium to stainless steel for UHV applications in superconducting cavities”, CERN/EF/RF 87-7, 1987.
- [14] J.D. Fuerst, W.F. Toter and K.W. Shepard, “Niobium to stainless steel braze transition development”, ANL, Argonne, IL 60439, USA.
- [15] L Leonel Marques Antunes Ferreira, Sergio Calatroni, Serge Forel (CERN, Geneva), Jamie Andrew Shirra (Loughborough University, Leicestershire), “Niobium Cavity Electropolishing Modelling And Optimisation”, these proceedings.
- [16] J. Chambrillon, “Cleanroom refurbishment in SM18 within the SPL project frame, feasibility study.”, sLHC Project note 0026, CERN, January 2011.